LANGMUIR

pubs.acs.org/Langmuir Article

Bulk Nanobubbles or Not Nanobubbles: That is the Question

Ananda J. Jadhav and Mostafa Barigou*

Cite This: *Langmuir* 2020, 36, 1699−1708 Read Online

ACCESS | Metrics & More | Article Recommendations | Supporting Information

ABSTRACT: Bulk nanobubbles are a novel nanoscale bubble system with unusual properties which challenge our understanding of bubble behavior. Because of their extraordinary longevity, their existence is still not widely accepted as they are often attributed to the presence of supramolecular structures or contaminants. Nonetheless, bulk nanobubbles are attracting increasing attention in the literature, but reports generally lack objective evidence that the observed nano-entities are indeed nanobubbles. In this paper, we use various physical and chemical analytical techniques to provide multiple evidence that the nano-entities produced mechanically in pure water by a continuous high-shear rotor-stator device or acoustic cavitation and spontaneously by water−ethanol mixing are indeed gas-filled domains. We estimate that the results presented here combined provide conclusive proof that bulk nanobubbles do exist and they are stable. This paper should help close the debate about the existence of bulk nanobubbles and, hence, enable the scientific community to rather focus on developing the missing fundamental science in this area.

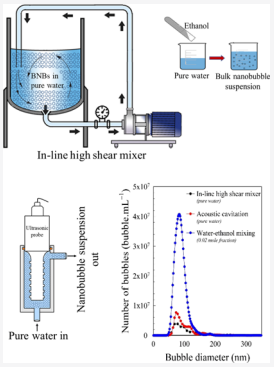

INTRODUCTION

Bulk nanobubbles are a novel nanoscale bubble system with unusual properties which challenge our understanding of bubble behavior. Their existence has been reported in many recent experimental studies, and they have also been the subject of a number of computational modeling studies. Diverse methods have been used to produce bulk nanobubbles including acoustic cavitation,[1−3] microfluidics,[4] electrolysis,[5−9] water solvent mixing,[3,10−12] pressure induced supersaturation,[13−15] and periodic pressure change method.[16] Bulk nanobubbles have been reported to exhibit long-term stability despite their very high inner pressure estimated from the Young−Laplace equation,[2,13,17,18] and various theories have been proposed to explain such extraordinary longevity.[19,20] However, reports are in the main conflicting and have not been independently validated, so there is no universally accepted theory that explains the existence and stability of bulk nanobubbles. For example, it has been speculated that nanobubbles are stable because of "universal" contamination, that is, each nanobubble is protected by a shell of insoluble contaminants (organic or surface-active molecules) which reduces the interfacial tension and hence the inner Laplace pressure, and provides stability against dissolution. The most interesting theory perhaps is the ion-stabilized model proposed by Bunkin et al.[21] It conjectures that the presence of negative electrostatic pressure because of adsorption of OH^- ions in the form of an electric double layer at the nanobubble interface, akin to that observed around solid nanoparticles, balances the internal Laplace pressure and, therefore, no net diffusion of gas occurs.[3]

Bulk nanobubbles have already attracted a lot of attention and various industrial and medical applications have been suggested.[17,22−30] However, despite such wide interest, this is still an emerging field and speculation remains rife about the existence of bulk nanobubbles and their stability as definite proof that the nano-entities observed are actually gas bubbles is still missing.[2,13,14,22,31] There is no technique available that combines high spatial resolution with chemical sensitivity to confirm whether the observed nano-entities are truly gas nanobubbles or rather nanoscale contamination. A number of authors have questioned the interpretation of the observed nano-objects as gas-filled nanobubbles often based on questionable experimentation and/or sheer speculation.[32−38] In mixtures of water and organic liquids, doubt exists as to whether the nano-entities observed are nanobubbles, supramolecular structures, or simply impurities.[32,39] Similarly, when generating bulk nanobubbles in pure water, another question that often arises is whether such nano-entities are oil droplets or solid nanoparticles which have detached from adjacent solid surfaces.[2,4,35]

In this paper, we use different mechanical and chemical techniques [continuous high-shear rotor-stator (HSRS) device, acoustic cavitation, and water−ethanol mixing] to generate bulk nanobubbles. These techniques, between them, encompass the main possible sources of contamination behind the controversy in the literature. We then use various physical and chemical analytical techniques to provide multiple evidence that bulk nanobubbles do exist and are stable in pure water and in aqueous ethanol solutions, as follows:

Received: November 13, 2019
Revised: December 19, 2019
Published: February 10, 2020

https://dx.doi.org/10.1021/acs.langmuir.9b03532
Langmuir 2020, 36, 1699−1708

(i) by showing that the amount of dissolved gas has a direct bearing on the number of nanobubbles generated using acoustic cavitation or water−ethanol mixing;
(ii) by separating ethanol from a water−ethanol nanobubble suspension and analyzing the nanobubble size distribution and bubble number density to confirm whether they are unaffected;
(iii) by monitoring the long-term stability of bulk nanobubbles and their gradual disappearance over time;
(iv) by complete evaporation of water and ethanol from nanobubble suspensions and examination of any residue;
(v) by using Fourier transform infrared spectroscopy (FT-IR) to analyze and compare the functional groups present in pure water and nanobubble suspensions;
(vi) by using Raman spectroscopy to analyze and compare the chemical composition and evaluate the strength of hydrogen bonding in pure water and nanobubble suspensions;
(vii) by analyzing pure water and nanobubble suspensions using gas chromatography mass spectroscopy (GC−MS) to analyze for any organic contamination;
(viii) by analyzing pure water and nanobubble suspensions using inductive coupled plasma mass spectroscopy (ICP−MS) to analyze for any inorganic contamination;
(ix) by studying the effect of freezing and thawing on nanobubble suspensions;
(x) by visualizing the nanobubbles as cavities using cryogenic scanning electron microscopy (Cryo-SEM);
(xi) by encapsulating the nanobubbles in a zinc phosphate shell and visualizing them as hollow nanoparticles using transmission electron microscopy (TEM).

EXPERIMENTAL SECTION

Materials. Ultrapure water (type-1), henceforth referred to as simply pure water, from a Millipore purification system (Avidity Science, UK), with an electrical conductivity of 0.055 $\mu S \cdot cm^{-1}$ and a pH of 6.7 at a temperature of 20 °C, was used in all experiments. All solvents and reagents used were of the highest purity grade available on the market. All glassware was cleaned by immersion for 30 min in a 10% aqueous solution of potassium hydroxide (KOH, Sigma-Aldrich, UK) placed inside an ultrasonic bath, followed by rinsing with ultrapure water, drying in a microwave oven, and flushing with a stream of high-purity dry nitrogen gas. Analytical grade ethanol (99.9% pure) used in experiments was procured from Fisher Scientific (UK). Prior to experimentation, purified water and all stock solutions were initially examined for any nanoscale entities using the Nanosight instrument (described further below) employed for the measurement of bulk nanobubbles, and no detectable levels of impurity were observed.

Methods of Generation of Bulk Nanobubble Suspensions. We used three different techniques to generate bulk nanobubble suspensions, namely, a continuous HSRS, acoustic cavitation, and water-solvent mixing. These techniques between them cover the typical sources of possible contamination including nanoparticles, oil, or solvent nanodroplets and supramolecular structures, as discussed above, that have been associated in the literature with the observation of nano-entities which are at the center of the bulk nanobubble debate.

Continuous HSRS Device. The working mechanisms of the HSRS device are based on the generation of high shear, intense turbulence, collision effects, and most importantly hydrodynamic cavitation which is probably responsible for the formation of microbubbles which shrink to form bulk nanobubbles, or may lead directly to the formation of nanobubbles. Bulk nanobubbles were generated using a continuous HSRS device (Silverson Machines Ltd, UK), as schematically represented in Figure S1A. The device was equipped with a single 4-blade rotor of 26 mm inner diameter and 38 mm outer diameter, located inside a stator of 39 mm inner diameter and 41 mm outer diameter having 8 holes of 10 mm diameter. The rotor was driven by a 1 hp (0.75 kW) variable speed motor with a maximum speed of 10 000 rpm. The experimental setup was used to generate 10 L of bulk nanobubble suspension by recirculating pure water for 30 min inside a 20 L stainless steel vessel at a fixed rotor speed of 10 000 rpm.

Acoustic Cavitation. Acoustic cavitation, like hydrodynamic cavitation HSRS, involves the generation, expansion, growth, and adiabatic collapse of microscopic cavities or microbubbles. Whilst microbubbles have always been assumed to collapse and vanish, here we presume that the disappearance of such microbubbles gives rise to the formation of nanobubbles which previously went undetected. However, it may also be possible that such nanobubbles are generated directly via cavitation. Bulk nanobubbles were generated by acoustic cavitation using a 20 kHz probe-type processor (AUTOTUNE SERIES 1500 W model, Sonics & Materials), as depicted in Figure S1B. A titanium probe of 1 inch diameter and 9 inch length was used to sonicate pure water flowing at a rate of 120 $mL \cdot min^{-1}$ through a 400 mL jacketed stainless steel cell, using a power of 188 W. The temperature of the sample was controlled at 20 °C by using a recirculating cooler (JULABO GmbH, Germany). Sonication was carried out for 5 min using a pulse mode of 5 s ON, 5 s OFF, equivalent to a total ultrasound exposure time of 100 s. The total volume of the nanobubble suspension generated was 1000 mL. Experiments were initially conducted at atmospheric pressure in continuous mode. To check the dependence of nanobubble generation on the availability of dissolved gas in water, using a rotary vacuum evaporator (RV 8 V-C, IKA, UK) as illustrated in Figure S2, pure water was first degassed for 5 h at a vacuum pressure of 10 mbar and acoustic cavitation was then applied in batch mode under these vacuum conditions using the same pulse mode for the same duration.

Water−Ethanol Mixing. Mixing of solvents such as ethanol and water equilibrated with atmospheric gases leads to supersaturation of dissolved gases which are less soluble in the mixture than in the individual components, thus, leading to possible nucleation of bulk nanobubbles. Here, bulk nanobubbles were generated by mixing ethanol with pure water at various mole fractions, X, at room temperature and atmospheric pressure in 100 mL glass beakers, as schematically represented in Figure S1C. The nanobubble suspensions formed were then stored in 20 mL air-tight glass vials for further analysis. To check the dependence of nanobubble generation on the availability of dissolved gas in water and ethanol, using a rotary evaporator, both liquids were degassed for 5 h under a vacuum pressure of 20 mbar and a temperature of 0.1 °C, followed by mixing under the same conditions. To avoid the absorption of gas from the atmosphere, ethanol was first evaporated in situ at 20 mbar and 3 °C and the remaining ethanol-free solution was then examined under atmospheric conditions.

Characterization of Bulk Nanobubble Suspensions. The size distribution and the number density of bulk nanobubbles were measured using a nanoparticle tracking analysis (NTA) instrument (NanoSight NS300, Malvern-UK). NTA tracks the Brownian motion of nanoparticles and is ideally suited for real-time analysis of polydisperse systems ranging from 10 to 2000 nm in size and 10^7 to 10^9 particles per mL in concentration. It is superior to dynamic light scattering whose measurements are based on the intensity of scattered light and is, thus, biased toward large particles.[2] Standard suspensions of solid latex nanospheres were used to verify the accuracy and precision of the NTA system and to adjust the instrument settings accordingly, prior to the analysis of nanobubble samples. The zeta potential of the nanobubbles was measured using a Zetasizer Nano ZSP instrument (ZEN5600, Malvern-UK). These measurement techniques and their protocols are discussed in more detail in our recent papers.[2,3]

Physical and Chemical Analytical Techniques. Here, we describe the various physical and chemical analytical techniques used to establish the evidence for the existence of bulk nanobubbles in pure water and in aqueous ethanol solutions.

Ethanol Separation from Water−Ethanol Nanobubble Suspension Experiment. The aim of this experiment was to test what happens when ethanol is removed from a bulk nanobubble suspension produced by water−ethanol mixing. Ethanol separation was carried out at 50 °C

https://dx.doi.org/10.1021/acs.langmuir.9b03532
Langmuir 2020, 36, 1699−1708

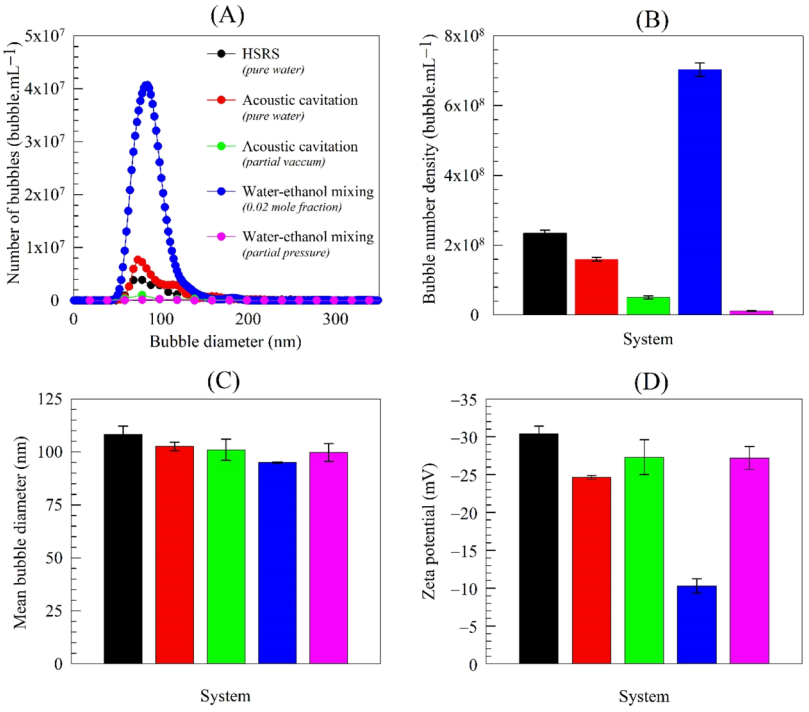

Figure 1. Characteristics of bulk nanobubbles obtained using different generation techniques under atmospheric pressure and partial vacuum showing effects of dissolved gas (day 1).

in a rotary vacuum evaporator using a vacuum (boiling) pressure of 291 mbar. The rotary evaporator experiments are schematically illustrated in Figure S2.

FT-IR Analysis. FT-IR is a nondestructive, quantitative, and quick method for identifying a wide range of chemical constituents and elucidating compound structures in various forms in real-world samples according to the vibrational modes of their molecular functional groups.[40] FT-IR spectroscopic measurements were used here to investigate the purity of bulk nanobubble suspensions produced in pure water and in water−ethanol. Spectroscopic measurements were performed on a Tensor 27 instrument (Bruker, Germany) coupled with an attenuated total reflection accessory. The scanned spectral range was from 400 to 4000 cm^{-1}, with a resolution of 2 cm^{-1} and a wavenumber accuracy of 0.01 cm^{-1}.

Raman Analysis. Raman spectroscopy is similar to FT-IR in that it also measures molecular vibrations to determine the chemical structure of a sample and identify the chemical compounds present.[41] Thus, Raman spectra provide a molecular fingerprint for identification and characterization of a given sample. In addition, they can give information on the strength of hydrogen bonding. It provides direct information on inter and intramolecular vibrational modes, which can be used to understand the interaction between water molecules and other materials (e.g., contamination). Raman spectroscopy data for pure water and bulk nanobubble suspensions were collected using an inVia Qontor Confocal Raman microscope (Renishaw, UK). Each scan had a 30 s acquisition time using a 532 nm laser at 10% power achieved using a pinhole aperture. Each spectrum was obtained using the average of three acquisitions between 100 and 4000 cm^{-1}.

GC−MS Analysis. GC−MS analysis of water and bulk nanobubble suspensions was performed with an Agilent 7890A gas chromatograph (Agilent Technology, UK) equipped with ZB-WAX column (30 m × ϕ 0.25 mm, thickness 0.25 μm, Phenomenex, UK) coupled to a GCT Premier mass spectrometer (Waters, UK) operated in electron ionization (EI$^+$) mode. Helium was used as a carrier and make-up gas passed through the column at a constant flowrate of 1.0 mL·min^{-1}. The injection volume was 1 μL, which was used with a split ratio of 1:10. The column temperature programme was as follows: temperature was held at 50 °C for 2 min, increased to 250 °C at 5 °C·min^{-1}, and then held at 250 °C for 18 min. The GC−MS operating parameters are summarized in Table S1.

ICP−MS Analysis. A NexION 300X ICP−MS spectrometer (PerkinElmer, UK) equipped with a cyclonic spray chamber and a SeaSpray concentric nebulizer was used to analyze pure water and bulk nanobubble suspensions for the presence of any trace metal particles. The ICP−MS operating parameters are summarized in Table S2. In order to quantify the analytical results of ICP−MS, the internal and external standard addition modes were used. All standards were prepared in 2% aqueous solution of HNO_3. Single element stock solutions (Sigma-Aldrich, UK) of 32 metals, namely, Na, Mg, Al, Si, P, K, Ca, Ti, V, Cr, Mn, Fe, Co, Ni, Cu, Zn, Rb, Sr, Zr, Ru, Rh, Pd, Ag, Cd, Sn, Sb, Te, Hf, Ir, Pt, Au, and Hg at a 1000 ppm concentration were used to prepare the standards for external calibration. The calibration curve and corresponding correlation coefficient (R^2 > 0.99) for each metal element used are presented in the Figures S3−S5. Indium at 1 ppm was employed as the internal standard. Pure water and bulk nanobubble suspensions were acidified using 2% HNO_3 prior to ICP−MS sampling. Samples were supplied to the nebulizer in continuous mode with the spectrometer peristaltic pump using flared end poly(vinyl chloride)-based tubing of 0.19 mm internal diameter.

Freezing and Thawing Experiments. Experiments were conducted to study what happens when bulk nanobubble suspensions of known bubble number density and mean bubble size are subjected to freezing at different temperatures followed by thawing at room temperature. Thus, 20 mL samples of nanobubble suspensions produced in pure water using the HSRS device or acoustic cavitation were kept in a freezer at −18 °C for a period of 24 h. Similarly, nanobubbles produced in water−ethanol mixtures were frozen in liquid nitrogen at −180 °C for 2 min, which exceeds the freezing point of pure ethanol to ensure that any ethanol in the mixture freezes. Subsequently, the frozen samples were left to thaw at room temperature for about 6 h before being analyzed by the NTA technique.

Cryo-SEM Analysis. Bulk nanobubbles in pure water were visualized using a Phillips XL30 FEG Cryo-SEM equipped with a Gatan low-temperature unit. The sample was prepared for Cryo-SEM by placing 1 μL of nanobubble suspension onto the copper holder and quenching it in liquid nitrogen at −180 °C under vacuum. Frozen specimens were transferred under a vacuum into an attached preparation chamber

https://dx.doi.org/10.1021/acs.langmuir.9b03532
Langmuir 2020, 36, 1699−1708

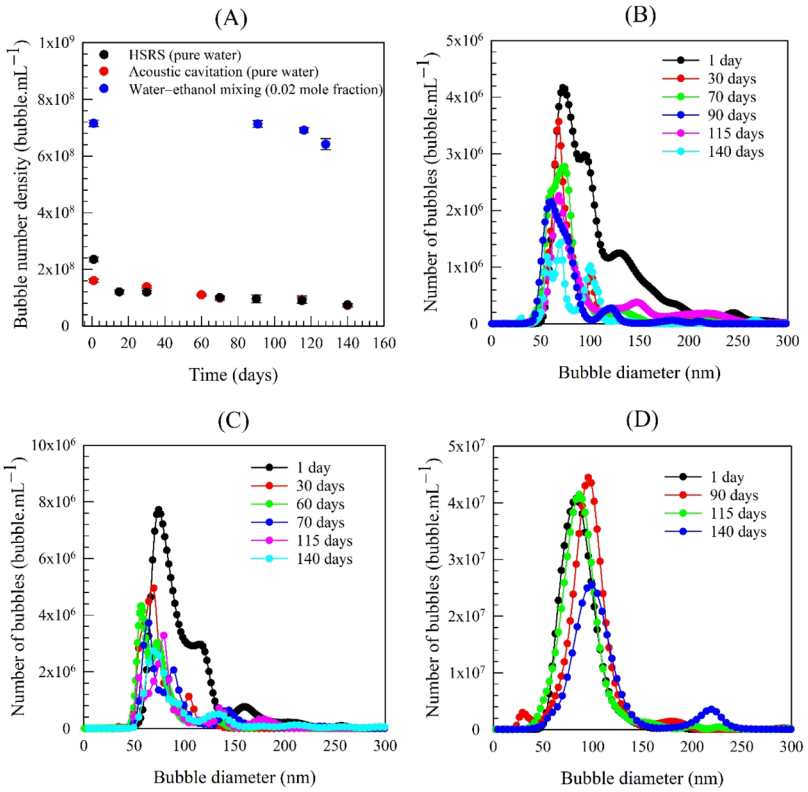

Figure 2. Long-term temporal evolution of (A) bubble number density and size distribution in different nanobubble suspensions: (B) HSRS; (C) acoustic cavitation; and (D) water−ethanol mixing.

where they were fractured with a cold scalpel blade, before being etched at −90 °C for 10 min and coated with sputtered gold. They were then transferred under a vacuum onto the cold stage and images were taken at a voltage of 5.0 kV to reduce temperature fluctuations associated with higher voltages, with the instrument maintained at −180 °C by the periodic addition of liquid nitrogen to the cooling chamber. For ease of visualization, we used a concentrated (by water evaporation in a vacuum rotary evaporator) bulk nanobubble suspension having a bubble number density of 1.39×10^{10} bubble·mL^{-1}; the mean bubble diameter was 104 nm.

Encapsulation of Nanobubbles and TEM Analysis. Bulk nanobubbles in pure water were used as a soft template for the synthesis of hollow zinc phosphate nanoparticles. To aid visualization of the hollow nanoparticles, the bulk nanobubble suspension which was prepared using the HSRS device was concentrated in a vacuum rotary evaporator. In a typical encapsulation procedure, using the concentrated nanobubble suspension, two separate 100 mL solutions, one containing 33.4 mM of zinc nitrate ($Zn(NO_3)_2{\cdot}6H_2O$), and the other 20 mM of diammonium phosphate ($(NH_4)_2HPO_4$), were prepared. The diammonium phosphate solution was slowly added to the zinc nitrate solution and the pH of the mixture was then adjusted to 8.5 with aqueous ammonia, resulting in the precipitation of white zinc-phosphate particles. The precipitate was collected by centrifugation, washed repeatedly with water and ethanol, and then dried in an oven at 40 °C for 12 h. The morphology of the synthesized particles was analyzed using a transmission electron microscope (TEM) (JEOL 2100 TEM, Japan) with an acceleration voltage of 200 kV. The TEM samples were prepared by depositing a few drops of the zinc phosphate nanoparticle suspending solution ultrasonically dispersed in ethanol on a carbon-coated gold grid.

RESULTS AND DISCUSSION

Characteristics of Bulk Nanobubble Suspensions. The characteristics, in terms of bubble size distribution, bubble number density, mean bubble diameter and zeta potential, of the bulk nanobubble suspensions generated by a continuous HSRS, acoustic cavitation, and water−ethanol mixing at atmospheric pressure are presented in Figure 1 together with results obtained under a partial vacuum. The five systems exhibit similar bubble size distributions and mean bubble diameter, but the bubble number density is higher for water−ethanol under atmospheric pressure. In pure water, the presence of a significant charge on the nanobubble interfaces seems to be responsible for their stability.[2,16] Indeed, nanobubbles produced in pure water via HSRS or acoustic cavitation have similar values of zeta potential (i.e., surface charge) which are much higher than that of the water−ethanol nanobubbles. This difference may be attributed to ethanol molecules adsorbing on the surface of the nanobubbles via hydrogen bonding, which reduces the magnitude of the zeta potential.[3,11,12] The ethanol separation experiments conducted further below confirm that the absence of ethanol restores the higher zeta potential found in pure nanobubble water.

Evidence for the Existence of Bulk Nanobubbles. We employed multiple physical and chemical analytical techniques to prove that the nano-entities produced by the different methods used here are indeed bubbles, as follows.

Effects of Dissolved Gas Content on the Formation of Nanobubbles. The acoustic cavitation and water−ethanol mixing experiments performed under a partial vacuum using a rotary vacuum evaporator, both show that the amount of dissolved gas greatly influences the number of nano-entities produced (see Figure 1). In both cases, there is about an order of magnitude reduction in nano-entities under a partial vacuum, which indicates that such nano-entities must be gas-filled.

Separation of Ethanol from Water−Ethanol Nanobubble Suspension. A rotary vacuum evaporation experiment (Figure

https://dx.doi.org/10.1021/acs.langmuir.9b03532
Langmuir 2020, 36, 1699−1708

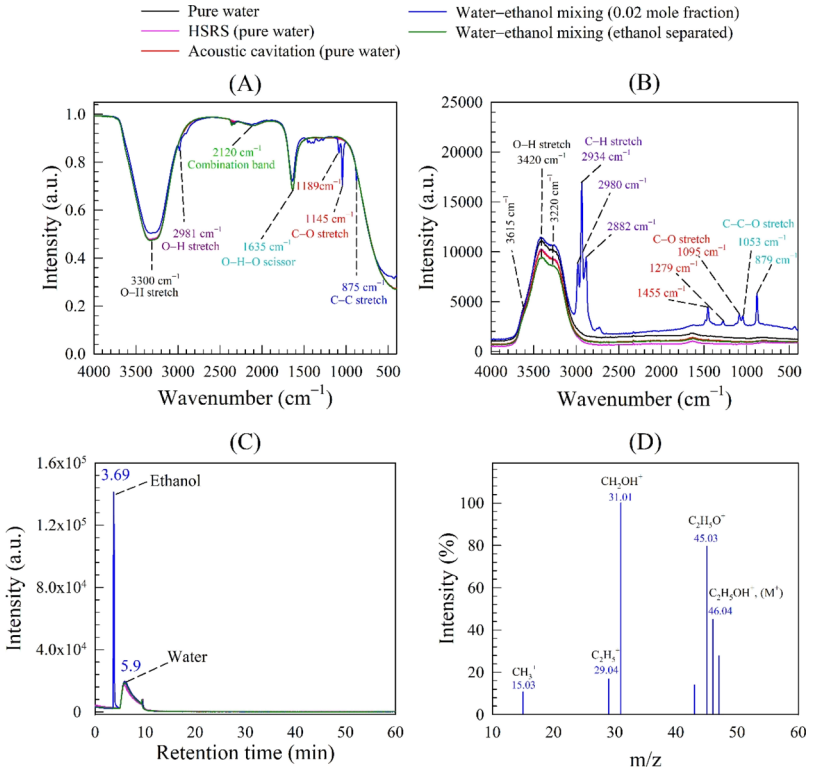

Figure 3. Spectroscopy analysis of nanobubble suspensions produced by different techniques in different systems: (A) FT-IR spectra; (B) Raman spectra; GC–MS results: (C) gas chromatogram; and (D) ethanol mass spectrum.

S2) was conducted to study what happens when ethanol is removed from a bulk nanobubble suspension produced by water–ethanol mixing. Separation of the entire ethanol content did not affect the size distribution or the bubble number density of the suspension. This result answers one of the important questions that the nano-entities produced during water–ethanol mixing are not ethanol droplets. The zeta potential measured in the ethanol-free nanobubble suspension was −26.5 mV (increasing in magnitude from −10.3 mV) which is approximately the same as for nanobubbles produced in pure water, as shown in Figure 1. This finding also indicates, as suggested above, that the ethanol molecules adsorb on the nanobubble interfaces via strong hydrogen bonding, which is confirmed further below when we measure the strength of hydrogen bonding in pure water and in water–ethanol mixtures using Raman spectroscopy.

Long-Term Stability of Bulk Nanobubbles. We monitored the long-term stability of the nanobubble suspensions by observing the evolution of their bubble number density, size distribution, mean bubble diameter, and zeta potential over long periods of time. Whilst the mean bubble diameter and zeta potential remained approximately unchanged (average values as shown in Figure 1), the bubble number density gradually reduced with time, as shown in Figure 2A. Most of the nanobubbles, however, were still stable after several months both in pure water and in the water–ethanol mixtures. The fact that the mean bubble size and the overall statistics of the size distribution remain constant over time (Figure 2B–D) does not only eliminate the possibility of (solid) particle agglomeration but it also suggests the absence of any significant effects arising from bubble coalescence, bubble breakage, or Ostwald ripening because of the strong surface charge. These results are entirely consistent with our recent reports.[2−4] The gradual disappearance of the observed nano-entities over time supports the belief that they are gas-filled bubbles.

Drying of Bulk Nanobubble Suspensions. Experiments were conducted to study what happens when a bulk nanobubble suspension of known bubble number density and mean bubble size is completely evaporated. Thus, 20 mL samples of nanobubble suspensions produced using our three different techniques were kept in glass flasks inside an oven at a temperature of 60 °C for a period of 24 h. After complete evaporation, the empty flasks were withdrawn from the oven and allowed to cool at room temperature for about 1 h, before adding 20 mL of ultrapure water. Any nonvolatile substance contained in the original nanobubble samples should have remained on the internal surface of the flasks. Each flask was gently agitated to suspend any such possible residue resulting from the evaporation process and the water then analyzed by the NTA technique. Typical results presented in Figure S6 show that, in all cases, no nano-entities were detected implying that the original samples contained no impurities and the observed nano-entities therein which disappeared during the evaporation process must have been bubbles.

FT-IR of Nanobubble Suspensions. FT-IR spectra are presented in Figure 3A for pure water and nanobubble suspensions produced in pure water by a continuous HSRS device or acoustic cavitation and by water–ethanol mixing. The FT-IR spectrum for pure water shows two intense bands at 3300 cm^{-1} and at 1635 cm^{-1} caused, respectively, by O–H stretching and O–H–O scissors bending. Furthermore, a smaller band is located at 2120 cm^{-1} which is the result of the coupling of the scissors-bending and a broad liberation band in the near infrared.[42] Any FT-IR detectable foreign substance would show as an extra peak. Because no extra peaks are observed in the pure water spectrum, it is safe to assume that the water used was free

https://dx.doi.org/10.1021/acs.langmuir.9b03532
Langmuir 2020, 36, 1699−1708

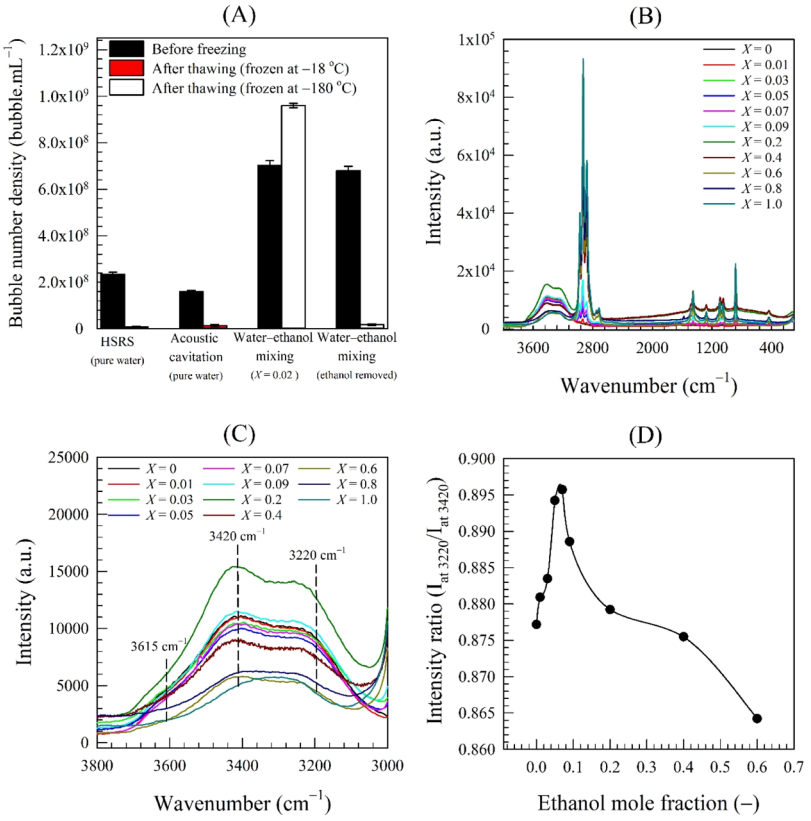

Figure 4. (A) Effects of freezing and thawing on nanobubble suspensions in different systems; and Raman spectra of nanobubble suspensions in different water−ethanol mixtures: (B) over range of wavenumbers from 100 to 3800 cm^{-1}; (C) over range of wavenumbers from 3000 to 3800 cm^{-1}; and (D) Raman intensity ratio ($I_{at\ 3200}/I_{at\ 3420}$) as a function of ethanol mole fraction.

from any detectable contamination. Moreover, the FT-IR spectra for the nanobubble suspensions produced in pure water coincide exactly with that of pure water (Figure 3A) which confirms that the nano-entities observed therein cannot be solid or liquid contamination.

The water−ethanol nanobubble suspensions in Figure 3A exhibit extra peaks representing the C−H stretching mode at 2981 cm^{-1}, the C−O stretching mode at 1189 and 1145 cm^{-1}, and the C−C stretching mode at 875 cm^{-1}, which together indicate the presence of ethanol, as expected. However, to confirm that these extra peaks do not mask the presence of other chemical compounds of similar functional groups, we conducted the same FT-IR analysis using water−ethanol nanobubble suspensions after complete separation of the ethanol content in the rotary evaporator. The extra peaks disappeared, and the corresponding FT-IR spectrum shown in Figure 3A now coincides with that of pure water. In conclusion, the FT-IR analysis confirmed that in all cases, the nano-entities observed in pure water or water−ethanol cannot be attributed to any type of FT-IR detectable contamination, strongly suggesting they must be gas/vapor-filled bubbles.

Raman Spectroscopy of Nanobubble Suspensions. Raman analysis spectra are presented in Figure 3B for pure water and nanobubble suspensions produced in pure water by HSRS or acoustic cavitation, and by water−ethanol mixing. The behavior of the Raman stretching band for pure water is similar to data reported by many authors,[43−45] including the distinctive three peaks at 3220, 3420, and 3615 cm^{-1}. The peak at 3220 cm^{-1} is attributed to the symmetric O−H stretching vibrational mode. The peak at 3420 cm^{-1} is attributed to the symmetric O−H stretching vibrational mode of asymmetrically bonded water molecules,[46] where the two Hydrogen atoms of water molecules are bonded to the neighboring water molecules by strong and weak hydrogen bonds, respectively. This peak strength is an indicator of bond disordering in the water molecular arrangement. The shoulder peak at 3615 cm^{-1} results from the free OH vibrational mode. The Raman spectra of the nanobubble suspensions produced in pure water by either HSRS or acoustic cavitation exhibit the same peaks as pure water.

The Raman spectrum of the water−ethanol nanobubble suspension exhibits extra peaks at 2934 and 2980 cm^{-1} which are attributed to the symmetric and asymmetric C−H stretching vibration modes, respectively. Other extra peaks represent the C−H stretching vibration mode at 2882 cm^{-1}, the wagging mode at 1455 cm^{-1}, the deformation wagging mode at 1279 cm^{-1}, the C−O stretching vibration mode at 1095 cm^{-1}, and the skeletal C−C−O deformation and stretching vibration modes, respectively, at 1053 and 879 cm^{-1}. All of these extra peaks confirm the presence of ethanol in the suspensions. Following the separation of ethanol by evaporation from the nanobubble suspension, all these extra peaks disappear and the spectrum coincides with that of pure water (Figure 3B). Thus, Raman analysis corroborates the FT-IR results and confirms that in all cases the nano-entities observed in pure water or in water−ethanol must be bubbles.

Gas Chromatography−Mass Spectrometry Analysis of Bulk Nanobubble Suspensions. It has been speculated that nanobubbles owe their stability to a protective shell of organic or surface active molecules,[19,47,48] whereas others have speculated that the observed nano-entities in pure water or water−ethanol were oil droplets.[33,34] Here, we use a GC−MS technique to specifically analyze our purified water and nanobubble

https://dx.doi.org/10.1021/acs.langmuir.9b03532
Langmuir 2020, 36, 1699−1708

suspensions for any organic contaminants. Results are presented in Figure 3C,D for pure water and all the nanobubble suspensions produced in pure water and water−ethanol. The gas chromatogram of pure water with a peak at a retention time of 5.9 min (Figure 3C) agrees with that reported by other workers.[49] The gas chromatograms of the nanobubble suspensions generated in pure water and of the water−ethanol nanobubble suspension after complete evaporation of ethanol, all coincide with that of pure water, which confirms that there is no organic contamination present. Similarly, the single peak at a retention time of 3.69 min represents the presence of ethanol in the water−ethanol nanobubble suspension, which has been confirmed using mass spectroscopy, as shown in Figure 3D.

Inductive Coupled Plasma-Mass Spectrometry Analysis of Bulk Nanobubble Suspensions. The concentrations of the 32 metal elements detected in the samples tested are given in Table S3. These results show that all of the nanobubble suspensions studied contained very low levels of metal traces similar to ultrapure water, which implies that the observed nano-entities could not be attributed to the presence of metal contamination.

Freezing and Thawing of Nanobubble Suspensions. The results of these freeze-thaw experiments are summarized in Figure 4A. After freezing and thawing, the bubble number density in pure water drops drastically below the resolution limit of the NTA instrument such that few nano-entities could be observed (see Video in Supporting Information). Hence, the nano-entities which have disappeared in pure water must be bubbles and could not be solid particles or droplets. It is hard to tell, however, whether the nanobubbles vanish during the freezing or thawing stage. Given that the freezing rate in pure water is very low, one could imagine that nanobubbles will be pressed to move and agglomerate or coalesce by the growing ice crystals in a way similar to the process of freeze concentration, leading eventually to rupture. This argument appears to be further supported by the Cryo-SEM results discussed below.

In contrast, the nanobubble suspension produced by water−ethanol mixing behaved strikingly differently, showing a higher bubble number density on thawing (Figure 4A). The cooling process of a water−ethanol mixture causes a significant increase in air supersaturation because of its enhanced solubility at low temperatures.[50,51] On thawing, as the temperature of the mixture rises, the solubility of air in the mixture diminishes, causing dissolved air to be spontaneously released from both water and ethanol and, hence, the formation of new nanobubbles. Consequently, two possible case scenarios could be envisaged: (i) it may be possible that the nanobubbles do actually vanish as in the case of pure water, but the presence of ethanol at low temperatures inevitably leads to the generation of a new more concentrated suspension of nanobubbles; or (ii) we argued above that ethanol molecules adsorb on the surface of nanobubbles via hydrogen bonding, which is reflected in their low zeta potential.[3] The adsorbed ethanol molecules should, thus, provide a thick protective shell that shields the nanobubbles and prevents them from collapsing on thawing, but the low temperatures lead to the creation of a nanobubble surplus.

To test the hypothesis of ethanol adsorption on nanobubble interfaces, we completely removed in a rotary evaporator the ethanol present in a nanobubble suspension generated by water−ethanol mixing. When the suspension was subsequently frozen and then thawed, the nanobubble concentration became vanishingly small in the same way as in the freezing and thawing of nanobubble suspensions in pure water (Figure 4A).

To provide further evidence, we used Raman spectroscopy to test the hypothesis of hydrogen bonding in the context of bulk nanobubbles. We measured the strength of hydrogen bonding in nanobubble suspensions obtained by mixing ethanol in water at various mole fractions, X, in the range 0−1. The Raman spectra corresponding to these nanobubble suspensions are presented in Figure 4B. The stretching lines of CH-groups apparent in the region 2800−3000 cm^{-1} precede the relatively extremely wide and nonhomogeneously broadened band of OH-groups of ethanol and water molecules spreading from 3000 to 3800 cm^{-1}. Upon increasing ethanol concentration in the solution, the OH band undergoes changes not only in its integral intensity but also in the contour shape, and the weak shoulder peak at 3615 cm^{-1} (free OH) disappears at a mole fraction of about 0.07 (Figure 4C). Using the intensity ratio of the O−H stretching band taken at 3220 and 3420 cm^{-1}, we evaluate the strength of H-bonding.[52] The value of the intensity ratio plotted in Figure 4D goes through a maximum, as expected, at an ethanol mole fraction of ∼0.07. The formation of hydrogen bonds between ethanol and water may be explained by referring to the enthalpy of formation/weakening of hydrogen bonds. Dolenko et al.[43] calculated the enthalpy of formation/weakening of the hydrogen bonds in pure water and in aqueous ethanol solutions of various concentrations. They found that the highest value of such enthalpy corresponded to an ethanol concentration of ∼20% v/v (i.e., ∼0.07 mole fraction) and the appearance of clathrate-like structures. At such a concentration, the hydrogen bonding is strongest between OH groups of water molecules and between molecules of water and ethanol in the ethanol hydrates.

The above findings confirm the adsorption of ethanol molecules and the strong hydrogen bonding at nanobubble interfaces. The presence of strong hydrogen bonds near the interface compensates for the lower surface charge and may be the prime factor in stabilizing bulk nanobubbles in a water−ethanol mixture.[3]

Cryo-Scanning Electron Microscopy. Cryo-SEM micrographs of pure water and a nanobubble suspension produced in pure water captured at different magnifications are presented in Figure 5. A smooth area of ice crystallites is observed in the case of pure water (Figure 5A,B). In the case of the nanobubble suspension, the ice surface contains numerous holes ranging from approximately 500−1000 nm in size (Figure 5C,D). This is

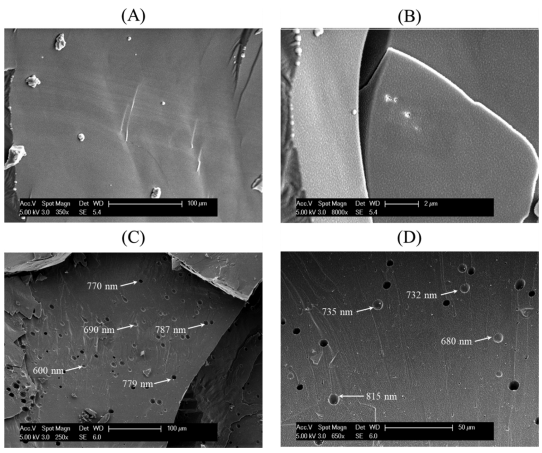

Figure 5. Cryo-SEM micrographs of pure water at magnifications of (A) 350, (B) 8000; and of bulk nanobubbles at magnifications of (C) 250 and (D) 650.

https://dx.doi.org/10.1021/acs.langmuir.9b03532
Langmuir 2020, 36, 1699−1708

clear physical evidence that the nano-entities present in the suspension are gas-filled cavities. The observed holes are much larger than the mean diameter of the original nanobubbles in the suspension, which suggests that the nanobubbles have agglomerated or coalesced during the freezing process. Thus, it appears that during freezing, nanobubbles give rise to much larger bubbles which may subsequently dissolve or disengage from the liquid during thawing by rising to the surface. This seems to provide a possible explanation for the disappearance of nanobubbles upon freezing and thawing of the suspension, as discussed above, and seems to corroborate the interpretation of the earlier observations.

Encapsulation of Nanobubbles and Analysis by TEM. Sample TEM images of the zinc phosphate nanoparticles are presented in Figure 6A,B. The core region of each particle

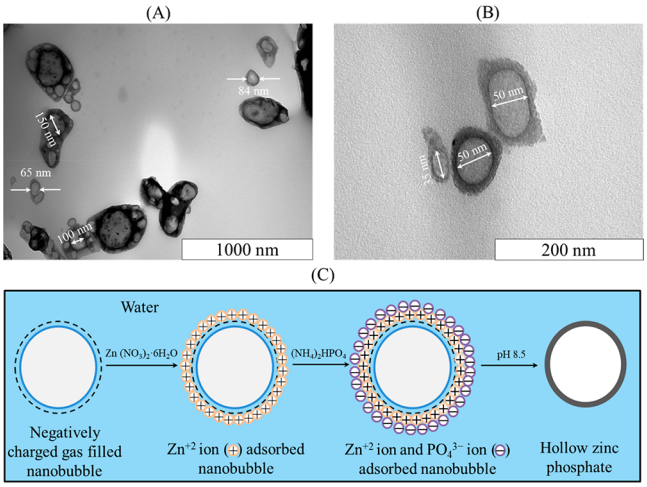

Figure 6. TEM images of hollow zinc phosphate nanoparticles obtained by encapsulation of bulk nanobubbles shown on different scales: (A) 1000; (B) 200 nm; and (C) schematic representation of the formation of the hollow nanoparticles.

appears brighter than the edge region, indicating that these particles are hollow with inner diameters ranging from 50 to 150 nm which are within the size range of the nanobubbles measured by NTA (Figure 1A). Thus, these hollow nanoparticles must have resulted from the encapsulation of bulk nanobubbles, again confirming that the nanobubbles are gas-filled and cannot be solid nanoparticles or nanodroplets. To ascertain this finding further, we carried out a parallel synthesis in pure water under identical experimental conditions. The morphologies of the two sets of zinc phosphate particles formed in pure water and in the nanobubble suspension were examined by SEM at room temperature and are compared in Figure S7. In pure water, the formed particles have a rod or sheet-like morphology on the micron scale, whereas in the nanobubble suspension they have a round oval shape and a size on the nanoscale. This confirms that the hollow nanoparticles obtained in the nanobubble suspension were formed by the encapsulation of nanobubbles, and that bulk nanobubbles can be used as a soft template for the formation of hollow-structured nanoparticles.

A schematic representation of the formation of the hollow zinc phosphate nanoparticles is presented in Figure 6C. Because bulk nanobubbles are negatively charged, Zn^{+2} ions from zinc nitrate adsorb on the nanobubble surfaces and provide nucleation sites for the subsequent reaction between Zn^{+2} and PO_4^{3-} ions from ammonium phosphate at pH 8.5. Thus, zinc phosphate precipitates on the nanobubble surfaces forming hollow particles.

CONCLUSIONS

We used various physical and chemical analytical techniques to show that the nano-entities observed in pure water or in water−ethanol are indeed gas-filled domains, that is, nanobubbles, by demonstrating that: (i) such nano-entities exhibit long-term stability but tend to gradually disappear over time; (ii) in a water−ethanol mixture, these nano-entities are not ethanol droplets; (iii) the amount of dissolved gas has a direct bearing on the number of nanobubbles generated; (iv) complete evaporation of water and solvent does not leave any residue; (v) all suspensions consist of the same functional groups as pure water; (vi) freezing and thawing causes all nano-entities suspended in water to disappear; (vii) the observed nano-entities cannot be attributed to the presence of any organic or inorganic impurities; (viii) in Cryo-SEM images, the nano-entities show as cavities; (ix) the encapsulation of the nano-entities with zinc phosphate produces hollow nanoparticles.

ASSOCIATED CONTENT

Supporting Information

The Supporting Information is available free of charge at https://pubs.acs.org/doi/10.1021/acs.langmuir.9b03532.

Schematics of the (A) continuous HSRS device; (B) acoustic cavitation setup and (C) water−ethanol mixing process, schematics of vacuum rotary evaporator experiments, calibration curves for individual elements measured by ICP−MS, bubble number density before and after complete evaporation of pure water and of nanobubble suspensions, SEM micrographs of zinc phosphate nanoparticles prepared in pure water and in the nanobubble suspension, GC−MS operating parameters, ICP−MS operating parameters, concentrations of elements in pure water and in nanobubble suspensions measured by ICP−MS (PDF)

Sample video of bulk nanobubbles before freezing and after thawing (MP4)

AUTHOR INFORMATION

Corresponding Author

Mostafa Barigou − *School of Chemical Engineering, University of Birmingham, Birmingham B15 2TT, U.K.*; orcid.org/0000-0003-0850-4011; Email: m.barigou@bham.ac.uk

Author

Ananda J. Jadhav − *School of Chemical Engineering, University of Birmingham, Birmingham B15 2TT, U.K.*

Complete contact information is available at: https://pubs.acs.org/10.1021/acs.langmuir.9b03532

Notes

The authors declare no competing financial interest.

ACKNOWLEDGMENTS

This work was supported by EPSRC grant EP/L025108/1.

REFERENCES

(1) Yasuda, K.; Matsushima, H.; Asakura, Y. Generation and Reduction of Bulk Nanobubbles by Ultrasonic Irradiation. *Chem. Eng. Sci.* **2019**, *195*, 455−461.

(2) Nirmalkar, N.; Pacek, A. W.; Barigou, M. On the Existence and Stability of Bulk Nanobubbles. *Langmuir* **2018**, *34*, 10964−10973.
(3) Nirmalkar, N.; Pacek, A. W.; Barigou, M. Bulk Nanobubbles from Acoustically Cavitated Aqueous Organic Solvent Mixtures. *Langmuir* **2019**, *35*, 2188−2195.
(4) Nirmalkar, N.; Pacek, A. W.; Barigou, M. Interpreting the Interfacial and Colloidal Stability of Bulk Nanobubbles. *Soft Matter* **2018**, *14*, 9643−9656.
(5) Kikuchi, K.; Nagata, S.; Tanaka, Y.; Saihara, Y.; Ogumi, Z. Characteristics of Hydrogen Nanobubbles in Solutions Obtained with Water Electrolysis. *J. Electroanal. Chem.* **2007**, *600*, 303−310.
(6) Kikuchi, K.; Ioka, A.; Oku, T.; Tanaka, Y.; Saihara, Y.; Ogumi, Z. Concentration Determination of Oxygen Nanobubbles in Electrolyzed Water. *J. Colloid Interface Sci.* **2009**, *329*, 306−309.
(7) Chen, Q.; Wiedenroth, H. S.; German, S. R.; White, H. S. Electrochemical Nucleation of Stable N2 Nanobubbles at Pt Nanoelectrodes. *J. Am. Chem. Soc.* **2015**, *137*, 12064−12069.
(8) Chen, Q.; Luo, L.; White, H. S. Electrochemical Generation of a Hydrogen Bubble at a Recessed Platinum Nanopore Electrode. *Langmuir* **2015**, *31*, 4573−4581.
(9) Chen, Q.; Luo, L.; Faraji, H.; Feldberg, S. W.; White, H. S. Electrochemical Measurements of Single H2 Nanobubble Nucleation and Stability at Pt Nanoelectrodes. *J. Phys. Chem. Lett.* **2014**, *5*, 3539−3544.
(10) Qiu, J.; Zou, Z.; Wang, S.; Wang, X.; Wang, L.; Dong, Y.; Zhao, H.; Zhang, L.; Hu, J. Formation and Stability of Bulk Nanobubbles Generated by Ethanol−Water Exchange. *ChemPhysChem* **2017**, *18*, 1345−1350.
(11) Millare, J. C.; Basilia, B. A. Dispersion and Electrokinetics of Scattered Objects in Ethanol-Water Mixtures. *Fluid Phase Equilib.* **2019**, *481*, 44−54.
(12) Millare, J. C.; Basilia, B. A. Nanobubbles from Ethanol-Water Mixtures: Generation and Solute Effects via Solvent Replacement Method. *ChemistrySelect* **2018**, *3*, 9268−9275.
(13) Ohgaki, K.; Khanh, N. Q.; Joden, Y.; Tsuji, A.; Nakagawa, T. Physicochemical Approach to Nanobubble Solutions. *Chem. Eng. Sci.* **2010**, *65*, 1296−1300.
(14) Oh, S. H.; Kim, J.-M. Generation and Stability of Bulk Nanobubbles. *Langmuir* **2017**, *33*, 3818−3823.
(15) Ushikubo, F. Y.; Furukawa, T.; Nakagawa, R.; Enari, M.; Makino, Y.; Kawagoe, Y.; Shiina, T.; Oshita, S. Evidence of the Existence and the Stability of Nano-Bubbles in Water. *Colloids Surf., A* **2010**, *361*, 31−37.
(16) Wang, Q.; Zhao, H.; Qi, N.; Qin, Y.; Zhang, X.; Li, Y. Generation and Stability of Size-Adjustable Bulk Nanobubbles Based on Periodic Pressure Change. *Sci. Rep.* **2019**, *9*, 1−9.
(17) Ebina, K.; Shi, K.; Hirao, M.; Hashimoto, J.; Kawato, Y.; Kaneshiro, S.; Morimoto, T.; Koizumi, K.; Yoshikawa, H. Oxygen and Air Nanobubble Water Solution Promote the Growth of Plants, Fishes, and Mice. *PloS One* **2013**, *8*, No. e65339.
(18) Meegoda, J. N.; Aluthgun Hewage, S.; Batagoda, J. H. Stability of Nanobubbles. *Environ. Eng. Sci.* **2018**, *35*, 1216−1227.
(19) Yasui, K.; Tuziuti, T.; Kanematsu, W.; Kato, K. Dynamic Equilibrium Model for a Bulk Nanobubble and a Microbubble Partly Covered with Hydrophobic Material. *Langmuir* **2016**, *32*, 11101−11110.
(20) Meegoda, J. N.; Hewage, S. A.; Batagoda, J. H. Application of the Diffused Double Layer Theory to Nanobubbles. *Langmuir* **2019**, *35*, 12100−12112.
(21) Bunkin, N. F.; Shkirin, A. V.; Suyazov, N. V.; Babenko, V. A.; Sychev, A. A.; Penkov, N. V.; Belosludtsev, K. N.; Gudkov, S. V. Formation and Dynamics of Ion-Stabilized Gas Nanobubble Phase in the Bulk of Aqueous NaCl Solutions. *J. Phys. Chem. B* **2016**, *120*, 1291−1303.
(22) Agarwal, A.; Ng, W. J.; Liu, Y. Principle and Applications of Microbubble and Nanobubble Technology for Water Treatment. *Chemosphere* **2011**, *84*, 1175−1180.
(23) Temesgen, T.; Bui, T. T.; Han, M.; Kim, T.-i.; Park, H. Micro and Nanobubble Technologies as a New Horizon for Water-Treatment Techniques: A Review. *Adv. Colloid Interface Sci.* **2017**, *246*, 40−51.
(24) Hu, L.; Xia, Z. Application of Ozone Micro-Nano-Bubbles to Groundwater Remediation. *J. Hazard. Mater.* **2018**, *342*, 446−453.
(25) Cai, W. B.; Yang, H. L.; Zhang, J.; Yin, J. K.; Yang, Y. L.; Yuan, L. J.; Zhang, L.; Duan, Y. Y. The Optimized Fabrication of Nanobubbles as Ultrasound Contrast Agents for Tumor Imaging. *Sci. Rep.* **2015**, *5*, 13725.
(26) Du, J.; Li, X.-Y.; Hu, H.; Xu, L.; Yang, S.-P.; Li, F.-H. Preparation and Imaging Investigation of Dual-Targeted C 3 F 8 -Filled PLGA Nanobubbles as a Novel Ultrasound Contrast Agent for Breast Cancer. *Sci. Rep.* **2018**, *8*, 1−18.
(27) Wang, J.-P.; Zhou, X.-L.; Yan, J.-P.; Zheng, R.-Q.; Wang, W. Nanobubbles as Ultrasound Contrast Agent for Facilitating Small Cell Lung Cancer Imaging. *Oncotarget* **2017**, *8*, 78153−78162.
(28) Liu, S.; Oshita, S.; Makino, Y.; Wang, Q.; Kawagoe, Y.; Uchida, T. Oxidative Capacity of Nanobubbles and Its Effect on Seed Germination. *ACS Sustain. Chem. Eng.* **2016**, *4*, 1347−1353.
(29) Liu, S.; Kawagoe, Y.; Makino, Y.; Oshita, S. Effects of Nanobubbles on the Physicochemical Properties of Water: The Basis for Peculiar Properties of Water Containing Nanobubbles. *Chem. Eng. Sci.* **2013**, *93*, 250−256.
(30) Oh, S. H.; Han, J. G.; Kim, J.-M. Long-Term Stability of Hydrogen Nanobubble Fuel. *Fuel* **2015**, *158*, 399−404.
(31) Zhu, J.; An, H.; Alheshibri, M.; Liu, L.; Terpstra, P. M. J.; Liu, G.; Craig, V. S. J. Cleaning with Bulk Nanobubbles. *Langmuir* **2016**, *32*, 11203−11211.
(32) Sedlák, M.; Rak, D. Large-Scale Inhomogeneities in Solutions of Low Molar Mass Compounds and Mixtures of Liquids: Supramolecular Structures or Nanobubbles? *J. Phys. Chem. B* **2013**, *117*, 2495−2504.
(33) Alheshibri, M.; Craig, V. S. J. Differentiating between Nanoparticles and Nanobubbles by Evaluation of the Compressibility and Density of Nanoparticles. *J. Phys. Chem. C* **2018**, *122*, 21998−22007.
(34) Alheshibri, M.; Craig, V. S. J. Generation of Nanoparticles upon Mixing Ethanol and Water; Nanobubbles or Not? *J. Colloid Interface Sci.* **2019**, *542*, 136−143.
(35) Häbich, A.; Ducker, W.; Dunstan, D. E.; Zhang, X. Do Stable Nanobubbles Exist in Mixtures of Organic Solvents and Water? *J. Phys. Chem. B* **2010**, *114*, 6962−6967.
(36) Leroy, V.; Norisuye, T. Investigating the Existence of Bulk Nanobubbles with Ultrasound. *ChemPhysChem* **2016**, *17*, 2787−2790.
(37) Rak, D.; Ovadová, M.; Sedlák, M. (Non)Existence of Bulk Nanobubbles: The Role of Ultrasonic Cavitation and Organic Solutes in Water. *J. Phys. Chem. Lett.* **2019**, *10*, 4215−4221.
(38) Alheshibri, M.; Jehannin, M.; Coleman, V. A.; Craig, V. S. J. Does Gas Supersaturation by a Chemical Reaction Produce Bulk Nanobubbles? *J. Colloid Interface Sci.* **2019**, *554*, 388−395.
(39) Jin, F.; Ye, J.; Hong, L.; Lam, H.; Wu, C. Slow Relaxation Mode in Mixtures of Water and Organic Molecules: Supramolecular Structures or Nanobubbles? *J. Phys. Chem. B* **2007**, *111*, 2255−2261.
(40) Zhang, J.; Li, B.; Wang, Q.; Wei, X.; Feng, W.; Chen, Y.; Huang, P.; Wang, Z. Application of Fourier Transform Infrared Spectroscopy with Chemometrics on Postmortem Interval Estimation Based on Pericardial Fluids. *Sci. Rep.* **2017**, *7*. https://doi.org/ DOI: 10.1038/s41598-017-18228-7.
(41) Ferraro, J. R.; Nakamoto, K.; Brown, C. W. Chapter 1 - Basic Theory. In *Introductory Raman Spectroscopy*, 2nd ed.; Ferraro, J. R., Nakamoto, K., Brown, C. W., Eds.; Academic Press: San Diego, 2003; pp 1−94.
(42) Drost-Hansen, W. The Structure and Properties of Water. D. Eisenberg and W. Kauzmann. Oxford University Press, New York, 1969. Xiv + 300 Pp., Illus. Cloth, $10; Paper, $4.50. *Science* **1969**, *166*, 861.
(43) Dolenko, T. A.; Burikov, S. A.; Dolenko, S. A.; Efitorov, A. O.; Plastinin, I. V.; Yuzhakov, V. I.; Patsaeva, S. V. Raman Spectroscopy of Water−Ethanol Solutions: The Estimation of Hydrogen Bonding Energy and the Appearance of Clathrate-like Structures in Solutions. *J. Phys. Chem. A* **2015**, *119*, 10806−10815.
(44) Walrafen, G. E. Raman Spectral Studies of the Effects of Temperature on Water Structure. *J. Chem. Phys.* **1967**, *47*, 114−126.

(45) Dolenko, T. A.; Churina, I. V.; Fadeev, V. V.; Glushkov, S. M. Valence Band of Liquid Water Raman Scattering: Some Peculiarities and Applications in the Diagnostics of Water Media. *J. Raman Spectrosc.* **2000**, *31*, 863−870.
(46) Li, F.; Men, Z.; Li, S.; Wang, S.; Li, Z.; Sun, C. Study of Hydrogen Bonding in Ethanol-Water Binary Solutions by Raman Spectroscopy. *Spectrochim. Acta Mol. Biomol. Spectrosc.* **2018**, *189*, 621−624.
(47) Yasui, K.; Tuziuti, T.; Kanematsu, W. Mysteries of Bulk Nanobubbles (Ultrafine Bubbles); Stability and Radical Formation. *Ultrason. Sonochem.* **2018**, *48*, 259−266.
(48) Yasui, K.; Tuziuti, T.; Izu, N.; Kanematsu, W. Is Surface Tension Reduced by Nanobubbles (Ultrafine Bubbles) Generated by Cavitation? *Ultrason. Sonochem.* **2019**, *52*, 13−18.
(49) Mekala, M.; Goli, V. R. Data on Acetic Acid−Methanol−Methyl Acetate−Water Mixture Analysised by Dual Packed Column Gas Chromatography. *Data Brief.* **2018**, *18*, 947−960.
(50) Cargill, R. W. The Solubility of Gases in Water−Alcohol Mixtures. *Chem. Soc. Rev.* **1993**, *22*, 135−141.
(51) Tokunaga, J. Solubilities of Oxygen, Nitrogen, and Carbon Dioxide in Aqueous Alcohol Solutions. *J. Chem. Eng. Data* **1975**, *20*, 41−46.
(52) Burikov, S.; Dolenko, T.; Patsaeva, S.; Starokurov, Y.; Yuzhakov, V. Raman and IR Spectroscopy Research on Hydrogen Bonding in Water−Ethanol Systems. *Mol. Phys.* **2010**, *108*, 2427−2436.

https://dx.doi.org/10.1021/acs.langmuir.9b03532
Langmuir 2020, 36, 1699−1708